The EMBO Journal Vol.18 No.1 pp.9–21, 1999

Structural basis for the recognition of superantigen streptococcal pyrogenic exotoxin A (SpeA1) by MHC class II molecules and T-cell receptors

Anastassios C.Papageorgiou, Carleen M.Collins[1], Delia M.Gutman[1], J.Bradford Kline[1,2], Susan M.O'Brien[3], Howard S.Tranter[3] and K.Ravi Acharya[4]

Department of Biology and Biochemistry, University of Bath, Claverton Down, Bath BA2 7AY, UK, [1]Department of Microbiology and Immunology, University of Miami School of Medicine, Miami, FL 33101, USA and [3]Centre for Applied Microbiology Research, Porton Down, Salisbury SP4 0JG, UK

[2]Present address: Department of Pathology and Laboratory of Medicine, University of Pennsylvania, Philadelphia, PA 19104, USA

[4]Corresponding author
e-mail: K.R.Acharya@bath.ac.uk

Streptococcal pyrogenic exotoxin A (SpeA) is a superantigen produced by *Streptococcus pyogenes* and is associated with severe infections characterized by rash, hypotension, multiorgan failure and a high mortality rate. In this study, an allelic form of this toxin, SpeA1, was crystallized with four molecules in the crystallographic asymmetric unit and its crystal structure was determined at 2.6 Å resolution. The crystallographic *R*-factor was 19.4% (33 497 reflections) for 7031 protein atoms and 88 water molecules. The overall structure of SpeA1 is considerably similar to that of other prototype microbial superantigens, either of staphylococcal or streptococcal origin, but has greatest similarity to staphylococcal enterotoxin C (SEC). Based on structural and mutagenesis data, we have mapped several important residues on the toxin molecule, which are involved in the recognition of major histocompatibility complex (MHC) class II molecules and T-cell receptors. Also, the toxin appears to possess a potential zinc-binding site which may have implications in binding to particular MHC class II molecules. Finally, we propose models for SpeA1–MHC class II and SpeA1–T-cell receptor association and the relevance of this phenomenon to the superantigenic action of this toxin is considered.

Keywords: molecular recognition/protein crystallography/pyrogenic exotoxin/superantigen/zinc binding

Introduction

In recent years there has been an increase in the incidence of serious invasive infections due to *Streptococcus pyogenes* (group A streptococcus) in both Europe and North America (Musser *et al*., 1991, 1993; Hoge *et al*., 1993). Many of these infections result in streptococcal toxic shock syndrome (STSS), which is a life-threatening illness characterized by rash, hypotension, and multiorgan failure (Stevens, 1995). The bacterial superantigen streptococcal pyrogenic exotoxin A is produced by a large percentage of the streptococcal strains isolated from patients with STSS and is believed to be associated with the onset of this syndrome (Bohach *et al*., 1990; Hauser *et al*., 1991).

SpeA (M_r 25 787) belongs to a family of staphylococcal and streptococcal superantigens which includes the staphylococcal enterotoxins (SEs) A, B, C1–3, D, E, G, H, toxic shock syndrome toxin-1 (TSST-1), the streptococcal pyrogenic exotoxins (Spes) B, C, possibly F and streptococcal superantigen (SSA). Superantigens are able to simultaneously bind to major histocompatibility complex (MHC) class II molecules and the T-cell receptor (TcR), resulting in the stimulation of a large number of T-cells expressing specific Vβ subsets of the TcR repertoire. However, binding of superantigens to MHC class II molecules requires no prior processing and occurs outside the antigen-binding groove (Marrack and Kappler, 1990). Superantigen activation of T-cells leads to increased secretion of specific cytokines by lymphocytes and monocytes, accumulation of which can result in acute shock and illness characteristic of STSS (Herman *et al*., 1991). Therefore, the correlation between STSS and SpeA-producing strains of *S.pyogenes* is not surprising, as STSS is defined by symptoms classic of a superantigen-mediated syndrome.

X-ray crystallographic techniques have led to the elucidation of a number of superantigen structures: SEA (Schad *et al*., 1995); SEB (Swaminathan *et al*., 1992; Papageorgiou *et al*., 1998); SEC2 (Papageorgiou *et al*., 1995; Swaminathan *et al*., 1995); SED (Sundström *et al*., 1996), TSST-1 (Prasad *et al*., 1993; Acharya *et al*., 1994; Papageorgiou *et al*., 1996) and SpeC (Roussell *et al*., 1997). All of these toxins have a characteristic two-domain fold (N- and C-terminal domains) containing a β-barrel known as the 'oligosaccharide/oligonucleotide fold' at the N-terminal domain, a long α-helix that diagonally spans the centre of the molecule and a 'β-grasp motif' at the C-terminal domain (Papageorgiou and Acharya, 1997). Moreover, crystal structures of SEB and TSST-1 in complex with a MHC class II molecule (HLA-DR1) (Jardetzky *et al*., 1994; Kim *et al*., 1994) and those of SEC2/SEC3 in complex with a TcR Vβ chain (Fields *et al*., 1996) are also available. Despite this large amount of crystallographic information, many questions regarding the exact mode of superantigen function remain unanswered. Moreover, the presence of one zinc-binding site in SEA, SEC2, SED and two zinc-binding sites in SpeC have indicated different modes in the assembly of the MHC–superantigen–TcR tri-molecular complex. From these studies, it has become clear that despite their structural and functional similarities, each superantigen may have adopted a slightly different method of complex formation with the TcR and MHC class II molecules (for recent reviews see Papageorgiou and Acharya, 1997; Kotb, 1998; Li *et al*., 1998).

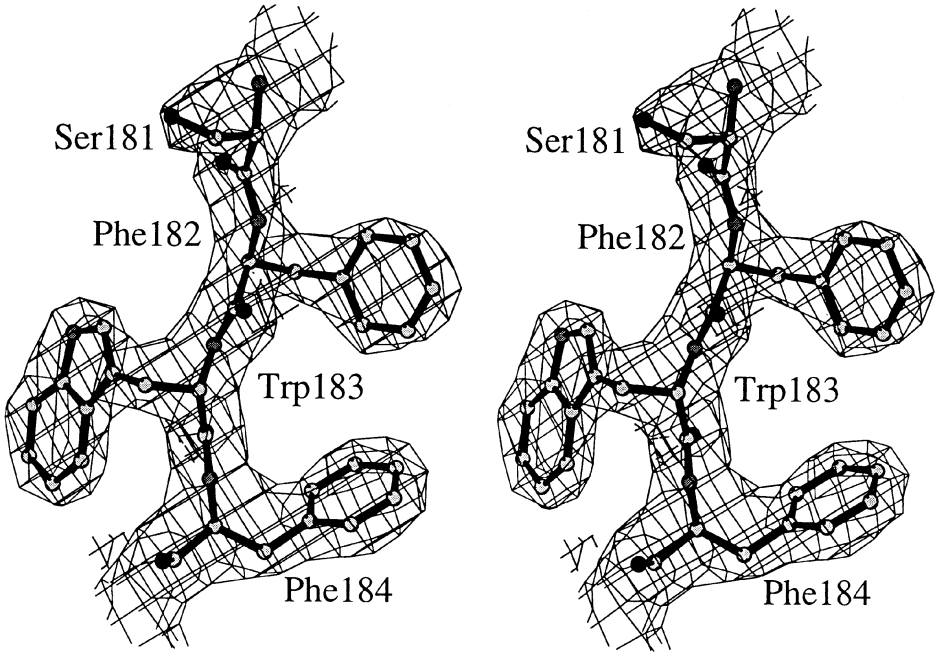

Fig. 1. Representative portion of the final 2 |Fo| – |Fc| electron density map of SpeA1 contoured at 1σ using the refined crystal structure at 2.57 Å resolution.

Four alleles of *speA* have been identified (*speA1*, *speA2*, *speA3* and *speA4*) (Nelson *et al*., 1991). The toxins encoded by *speA2* (SpeA2) and *speA3* (SpeA3) differ by a single amino acid substitution from the toxin encoded by *speA1* (SpeA1), while the toxin encoded by *speA4* (SpeA4) differs by 26 residues from SpeA1. Studies indicate that *speA2* and *speA3* are found in contemporary *S.pyogenes* isolates, while *speA1* is more often associated with strains recovered from earlier this century (Nelson *et al*., 1991; Musser *et al*., 1993). SpeA3 appears to be a more mitogenic form of the toxin than SpeA1 or SpeA2 (Kline and Collins, 1996). This may be because SpeA3 has a 10-fold higher affinity for the HLA-DQ molecule than SpeA1 (K_d = 10 nM compared with 100 nM). However, the reason for the difference in affinity for HLA-DQ is not known.

In order to better understand the superantigenic properties of SpeA, we have determined the crystal structure of SpeA1 at 2.6 Å resolution. This toxin has the characteristic 'superantigen fold' as has been observed for other members of the family. However, its binding to the TcR and MHC-class II molecules is likely to differ from other superantigens. Also, it possesses a putative zinc-binding site similar to that found in staphylococcal enterotoxin SEC2 (Papageorgiou *et al*., 1995).

Results and discussion

Quality of the structure

The three-dimensional crystal structure of SpeA1 was determined at 2.6 Å resolution (Figure 1). Details of the data collection and refinement statistics are shown in Table I. The protein crystallizes with four molecules per crystallographic asymmetric unit. The final model includes 7031 non-hydrogen protein atoms and 88 water molecules with a crystallographic *R*-factor (R_{cryst}) of 19.4% in the

Table I. Data processing and refinement statistics

Space group – orthorhombic $P2_12_12$; four molecules/asymmetric unit		
Cell dimensions (Å)	127.3×101.6×82.3	127.4×101.0×81.8
No. of crystals used	1	1
Resolution (Å)	40.0–2.9	20.0–2.57
No. of measurements	107 420	231 656
No. of unique reflections	23 581	33 531
Completeness (%)	95 (82.4)[a]	97.4 (84.5)[b]
$<I/\sigma(I)>$	5.9 (2.1)	8.6 (3.2)
R_{merge} (%) [c]	13.7 (51.6)	10.7 (42.8)
Refinement		
Resolution		20.0–2.57
No. of reflections [$F>0\sigma(F)$]		33 497
Protein atoms		7031
Water molecules		88
R_{cryst} (%)		19.4
R_{free} (%)		27.4
r.m.s. deviation		
Bond lengths (Å)		0.007
Bond angles (degree)		1.32
Dihedrals (degree)		28.30
Impropers (degree)		0.65
Thermal parameters (Å^2)		
Main chain		30.9 (26.6, 28.7, 23.2, 44.9)
Sidechain		31.2 (26.9, 28.8, 24.3, 44.7)
Water		24.9
B-factor (from Wilson plot)	57.0	41.4

[a]Outermost shell 3.0–2.9 Å.
[b]Outermost shell 2.70–2.57 Å.
[c]$R_{merge} = \Sigma(|I_j - <I>|)/\Sigma<I>$ where I_j is the observed intensity of reflection *j* and $<I>$ is the average intensity of multiple observations. Thermal parameters for individual molecules are quoted in brackets.

resolution range 20.0–2.57 Å. The last recorded R_{free} value was 27.4% for 5% of the reflections excluded from the refinement (Brünger, 1992a). The mean coordinate error calculated from a plot of $\ln\sigma_A$ versus $(\sin\theta/\lambda)^2$ is 0.26 Å (Read, 1986). The root mean square (r.m.s.) deviation in Cα atoms between monomer pairs is 0.32 (mol1–mol2), 0.26 (mol1–mol3) and 0.43 (mol1–mol4). Regions that deviate most include residues 3–8 from the N-terminal tail and part of the disulfide loop (residues 90–94). Exclusion of these regions from the calculations improves the r.m.s. deviation to 0.22 (mol1–mol2), 0.20 (mol1–mol3) and 0.25 Å (mol1–mol4). Examination of the Ramachandran plot (Laskowski *et al*., 1993) shows 84.1% of the residues (for the four molecules) in allowed regions and no residues in disallowed regions. The final electron density map for molecule 4 shows higher mobility in some regions. Residues 1–2 have not been modelled in all four molecules due to poor density. The extra four residues at the N-terminus resulting from the expression system used are highly flexible and not seen in the electron density map. Also, residues 5, 88, 107, 112, 115, 179 and 180 in all four molecules, and residues 91 and 92 in mol2, mol3 and mol4 have been modelled as alanines due to the lack of sufficient density beyond Cβ atoms. The arrangement of the four molecules and the nomenclature used throughout the text are shown in Figure 2A. Molecule 1 will be used throughout the discussion except where noted otherwise.

Overall structure

The topology of the SpeA1 molecule is remarkably similar to that of other superantigens (Figure 2B). It contains the central long α-helix, an N-terminal domain and a C-terminal domain. The two domains are closely packed and are connected by a stretch of five residues. The overall dimensions of the molecule are ~53×47×33 Å. Part of the N-terminal domain has a β-barrel topology formed by strands β1, β2, β3, β4 and β5, similar to the 'oligosaccharide/oligonucleotide fold' (Murzin *et al*., 1995) also present in other microbial superantigens. Strands β2 and β3 are antiparallel, and strand β1 is parallel to β5 and antiparallel to β4. Several hydrophobic residues from the β-barrel are solvent-exposed. Other structural features of the N-terminal domain include helices α2, α3 and α5 and a disulfide bridge in the β4–β5 loop. The C-terminal domain has features of the 'β-grasp motif' as observed in other known superantigen structures (Papageorgiou and Acharya, 1997) with a β-sheet topology packed against the central helix (α4). Strands β6, β9, β10 and β12 form a relatively flat surface with strand β7 rotated by ~30° with respect to β6. The N-terminal tail (residues 3–16) is packed against the β-grasp motif, hence it is considered as part of the C-terminal domain.

Comparison with other superantigen structures

SpeA1 (221 amino acids) is shorter than SEB (239 aa), SEC2 (239 aa) and SEA (235 aa) due to deletions in several loop regions. From the structural alignment (Figure 2C), it is clear that the overall structure of SpeA1 is most similar to SEC2 (Figure 3; Table II) when differences in αN–α2, α2–β1, β2–β3, the disulfide loop, β9–β10 and β11–β12 loop structures are excluded. In particular, the loop β2–β3 (residues 49–56) is much shorter than the corresponding loop in SEB (residues 53–62) and SEC2 (residues 54–61). This loop in SpeA1 contains a Gly-Pro motif (Gly52-Pro53) which results in a large r.m.s. deviation for this region (2.69 and 2.36 Å in comparison with SEC2 and SEB, respectively). A much larger r.m.s. deviation (~7 Å) in this region was observed when this molecule was compared with SEA. A second Gly-Pro motif in SpeA1 is found in the α4–β9 loop with an average deviation of ~1.3 Å for the corresponding residues in SEC2 (Asn-Ser) and SEB (Asn-Asn). These two motifs are located in loops implicated in TcR binding. Variability was also observed in the disulfide loop (see later sections). Portion of the N-terminal tail preceding the α2 helix also shows large deviations and the conserved glycine residue in SEB (Gly19), SEC2 (Gly19) and SEA (Gly20) is replaced by a basic amino acid (Lys16) in SpeA1.

The interface between the four molecules

Each monomer in SpeA1 has ≈10 600 Å^2 accessible surface area. Upon formation of mol1–mol2 or mol1–mol4 dimer, a loss of ~1400 Å^2 (~13%) of the accessible surface area of the monomer is observed, consistent with the results from other protein–protein interfaces. The interactions are mainly mediated through charged residues (Table III). Mol1 predominantly interacts with mol2 and mol4 and has relatively few interactions with mol3 (Figure 2A). Short hydrogen bond interactions occur between mol1 and mol2: Glu94 OE2–Gln194 N (2.57 Å), Gln194 N–Glu94 OE2 (2.53 Å); and between mol1–mol4: Ser43 OG–Glu191 N (2.74 Å), Glu191 N–Ser43 OG (2.81 Å) (Table IV).

Water molecules

A number of water molecules (88 in total) were identified with temperature factors <60 Å^2. Twenty-three of them are found in mol1, mol2 or mol3, and 19 in mol4. Five water molecules in mol1 are buried with temperature factors <15 Å^2. These water molecules are conserved in SpeA1 and in other known staphylococcal superantigen structures such as SEB and SEC2, and might play a structural role.

Disulfide bridge

The SpeA1 structure contains three cysteine residues; two of them (Cys87 and Cys98) form a disulfide bridge at the top of the N-terminal β-barrel, between strands β4 and β5 (Figure 2B and C). The third cysteine (Cys90) is accessible to solvent and is part of the disulfide loop. This loop is present in all the microbial superantigens except SpeC which does not contain any cysteine residue in the corresponding region and TSST-1 which does not possess any cysteine residues at all (Figure 2C). The SpeA1 disulfide loop is comprised of ten residues and is shorter than the corresponding loops in SEB and SEC which consist of 19 and 16 residues respectively, but is of similar length to that of SEA (nine residues) (Figure 2C). The residues of the disulfide loop in SpeA1 possess high temperature factors, indicative of high flexibility, and may adopt multiple conformations. In general, the high flexibility of the disulfide loop is a common feature in all SEs and hence increases the difficulty encountered in defining a single conformation for each of these toxins.

In the crystal structure of SpeA1 presented here, this loop has been identified at the interface between the four molecules, is therefore buried and involved in crystal packing interactions. However, it still retains some degree of flexibility, hence it is not surprising that superposition of the disulfide loop from the four molecules (residues 87–98) shows an r.m.s. deviation in Cα atoms of 0.52 (mol1–mol2), 0.27 (mol1–mol3) and 0.65 Å (mol1–mol4). The largest differences occur between residues 90–94, located in the middle of the loop. The role of the disulfide loop in superantigen recognition is discussed in later sections.

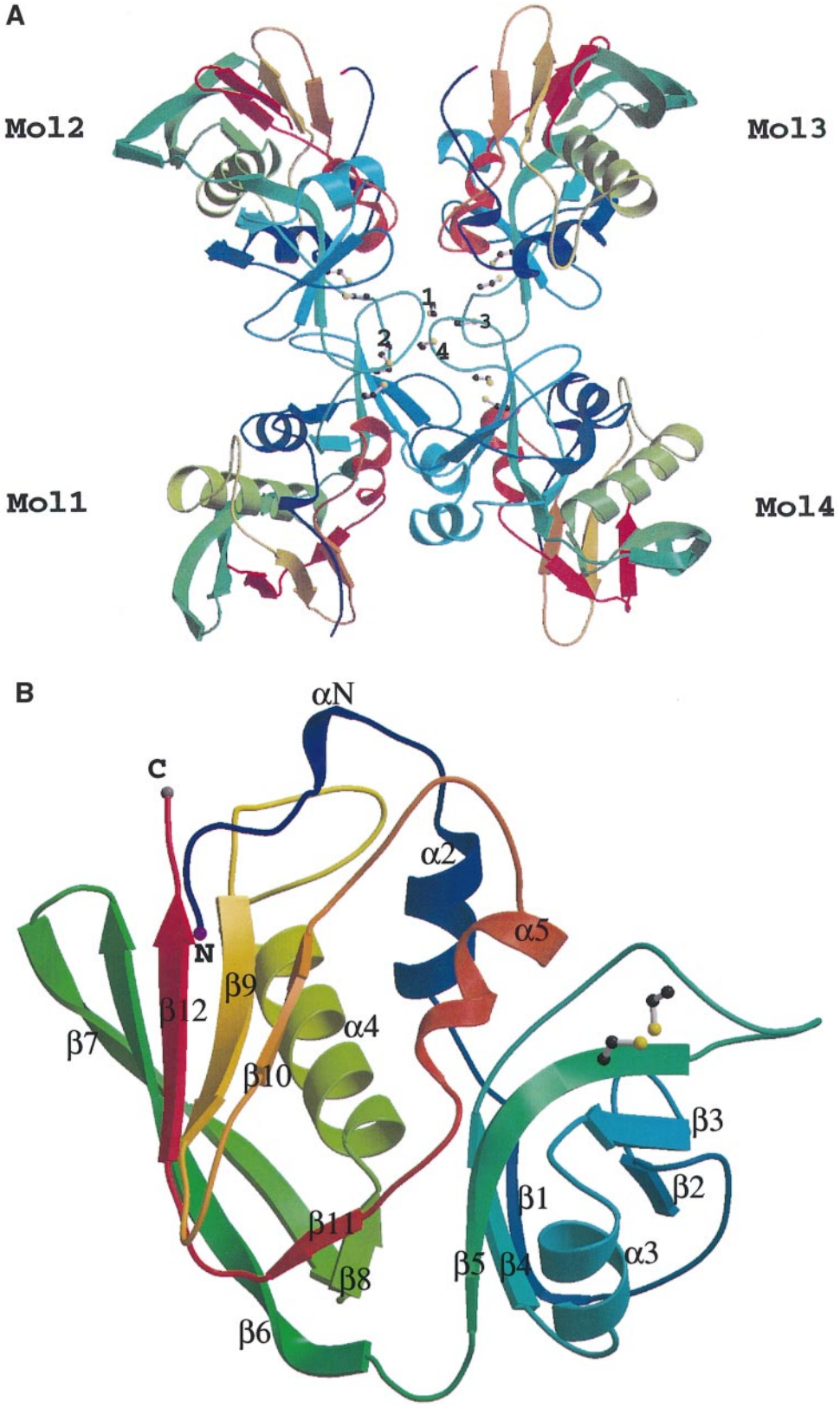

Potential zinc-binding site

The crystal structure of SpeA1 revealed the presence of a potential zinc-binding site formed by residues Asp77, His106 and His110 (Figure 2C). However, no zinc ion was found in this site. The toxin used to produce the crystals for this structure determination was purified with buffers at pH 5.7, and it is possible that at this low pH the zinc ion was removed from the binding site. In addition, it is possible that the metal ion was washed out during crystallization of the toxin. To investigate the

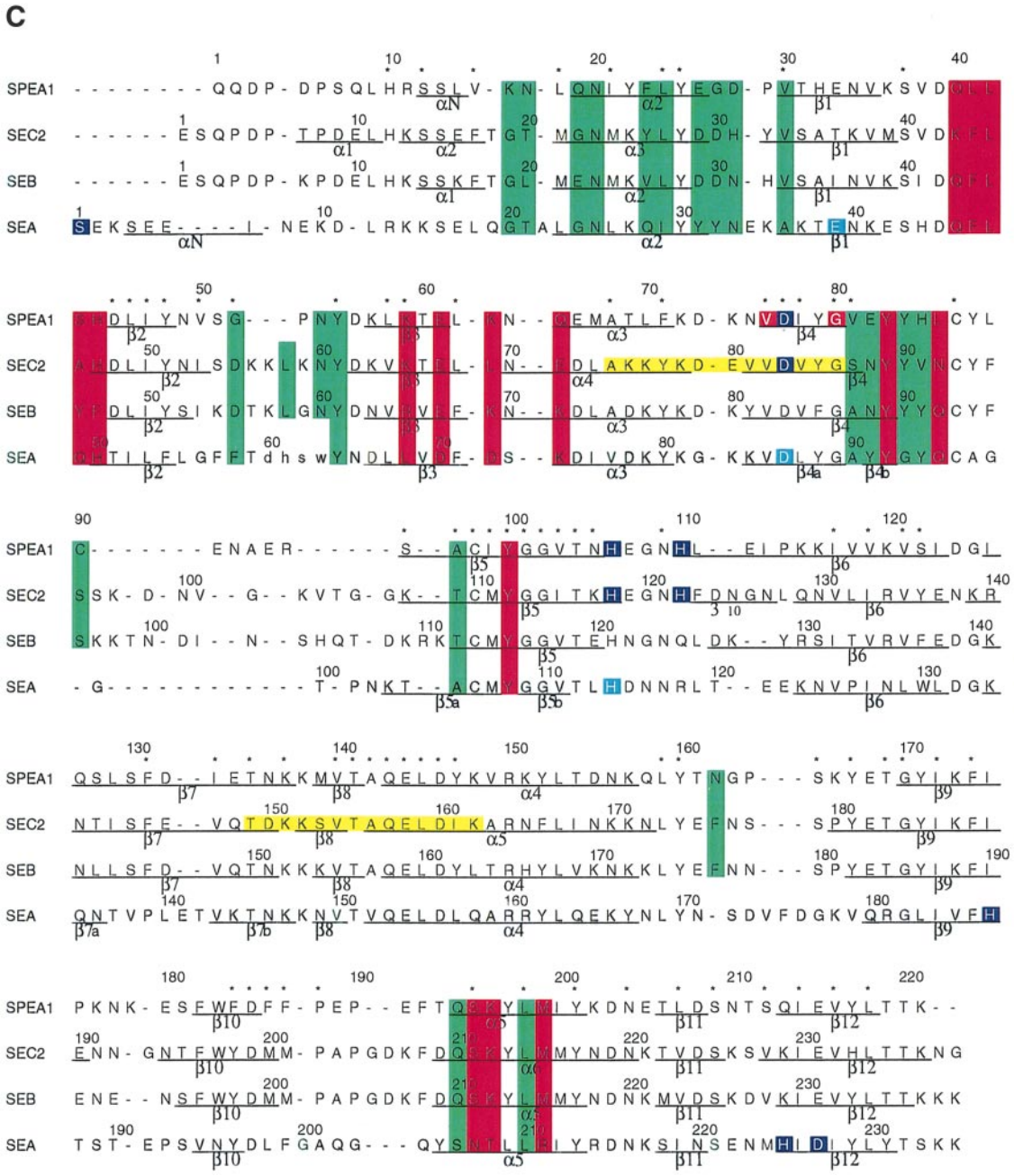

Fig. 2. (**A**) Arrangement of the four SpeA1 molecules in the crystallographic asymmetric unit. Each molecule is labelled. The intra-molecular disulfide bonds (Cys87–Cys98) are shown and the free cysteine (Cys90) in each molecule is labelled. The colour changing is from blue (N-terminus) to green (C-terminus). This figure was created with the program BOBSCRIPT (Esnouf, 1997). (**B**) Ribbon diagram of the SpeA1 molecule. The colour changing scheme is similar to that used in (A). The disulfide bond between residues 87 and 98 is shown. Secondary structure elements were assigned based on the program DSSP (Kabsch and Sander, 1983). The figure was created with the programs BOBSCRIPT (Esnouf, 1997) and Raster3D (Merritt and Murphy, 1994). (**C**) Structure-based sequence alignment of SpeA1, SEC2, SEB, SEA. Solvent inaccessible residues of SpeA1 (<20 Å^2 of exposed surface) are labelled with *. Every tenth residue is numbered. Secondary-structure elements are shown as determined by DSSP (Kabsch and Sander, 1983). Residues involved in MHC class II binding are coloured in red; those involved in TcR binding are in green. SEB residues Tyr89 and Gln92, and SpeA1 Cys87–Cys98 have been implicated in both interactions. Zinc ligands are shown in blue and those forming the second zinc-binding site in SEA in cyan (Schad *et al*., 1997). Residues of SpeA1 which differ in the two allelic forms of the toxin (SpeA2 and SpeA3) are shown in orange. Two SEC2 peptides proposed to bind MHC class II molecules are highlighted in yellow (Hoffmann *et al*., 1994). Residues of SEA in lower case have not been modelled in the structure and sequence alignment was used in this case. This figure was created with the program ALSCRIPT (Barton, 1993).

Fig. 3. Stereoview displaying the Cα traces of SpeA1 (solid line) and SEC2 (dashed line) after structural alignment of the two structures with the program SHP (Stuart *et al*., 1979).

presence of zinc ion in SpeA1, five distinct toxin preparations were analyzed for metal content by plasma emission spectroscopy. Four of these toxins were purified using pH 7.9 buffers and one was purified at pH 5.7. In all five toxin preparations there was one mole of zinc per mole of protein. Experiments to establish direct binding of zinc with in the crystal are currently in progress.

The residues of the predicted SpeA1 zinc-binding site (residues Asp77, His106 and His110) are structurally equivalent to residues Asp83, His118 and His122 in SEC2 (first proposed on the basis of sequence comparison and SEC2 crystal structure by Papageorgiou *et al*., 1995). Superposition of the SEC2 zinc-binding site and the corresponding site of SpeA1 shows remarkable similarity between the two (Figure 4). In the case of SEC2, the fourth zinc ligand was provided by Asp9 from a symmetry-related molecule brought into proximity due to crystal packing. In SpeA1, no crystal packing contacts occur in this region. However, a water molecule might provide an additional ligand for the coordination sphere and this can be verified once a high resolution structure of the toxin in the presence of zinc becomes available. Different and structurally non-equivalent zinc-binding sites have been identified in SEA (Schad *et al*., 1995), SED (Sundström *et al*., 1996) and SpeC (Roussell *et al*., 1997). Consequently, different possibilities for the role of the zinc-binding sites in superantigen binding to MHC class II molecules have been proposed (reviewed in Papageorgiou and Acharya, 1997).

MHC class II-binding site

It has been shown that SpeA1 competes with SEB for binding to DR molecules (Hartwig *et al*., 1994) and it is likely that these two toxins have a common recognition site for MHC class II molecules. However, SpeA1 and SEB have different affinities for MHC class II molecules. In particular, SpeA1, like SEC2, has a greater affinity for HLA-DQ than it does for HLA-DR or HLA-DP. In contrast, SEB has a greater affinity for HLA-DR. This suggests that the two toxins may have similar but not identical MHC-binding sites. A simple molecular modelling exercise where SpeA1 was superimposed onto DR1 using the coordinates of SEB from the SEB–DR1 complex (Jardetzky *et al*., 1994) revealed that nine of SpeA1 residues are similar to those of SEB which make contacts with the DR1 molecule (Figures 2C and 5). Moreover, Lys39 from DR1 (a key residue present in all three allotypes) forms a salt bridge with Glu67 in the SEB–DR1 complex. This glutamic acid residue is conserved in SpeA1 (Glu61 in Figure 2C) and SEC, but not in SEA and SED (Figure 2C). However, in order to understand the preference of SpeA1 to bind DQ molecules, it is necessary to investigate the sequence differences between DR and DQ and sequence differences between DR1-binding site of SEB and the analogous binding site of SpeA1.

Table II. R.m.s. deviation in Cα-atoms and sequence identity between different superantigens against SpeA1

	R.m.s.d. in Cα-atoms	Sequence identity (%)
SEC2–SpeA1	0.95	48.1
SEB–SpeA1	1.26	50.7
SEA–SpeA1	1.95	32.4
SpeC–SpeA1	2.44	27.6
TSST-1–SpeA1	2.85	19.9

Structure-based alignment was performed with the program SHP (Stuart *et al*., 1979). The sequence identity is deduced after the number of structurally equivalent residues is calculated.
R.m.s.d., root-mean-square deviation.

Table III. Contacts at mol1–mol2 and mol1–mol4 interfaces

Mol1	Mol2
Asn20	Glu94(1), Arg95(1)
Phe23	Arg95(12)
His85	Glu94(7), Ala93(1), Asn92(3), Glu91(3)
Glu91	His85(1)
Glu94	Asn20(1), His85(5), Thr193(5), Gln194(5)
Arg95	Asn20(1), Phe23(11)
Thr193	Glu94(3)
Gln194	Glu94(6)
Mol1	**Mol4**
Leu42	Glu191(3), Phe192(3), Lys196(1)
Ser43	Glu189(3), Pro190(4), Glu191(5)
His44	Glu189(1), Lys196(2)
Glu61	Lys196(3)
Gln65	His10(1), Glu189(3), Pro190(2)
Glu189	Ser43(2), His44(1), Gln65(3)
Pro190	Ser43(1), Gln65(3)
Glu191	Leu41(1), Leu42(3), Ser43(8)
Lys196	Leu42(1), His44(2), Glu61(2)

Contacts between different monomers were determined using the following criteria: maximum allowed values of C–C, 4.1 Å; C–N, 3.8 Å; C–O, 3.7 Å; O–O, 3.3 Å; O–N, 3.4 Å; N–N, 3.4 Å. Residues 91 and 92 have been modelled as Ala in mol2. The number of contacts are given in parentheses.

Previous studies have identified SpeA1 residues required for high affinity binding to HLA-DQ (Kline and Collins, 1996). Substitution of each of the SpeA1 residues Leu42, Asp45, Leu46, Ile47, Tyr48 and Tyr83 with alanine resulted in a significant decrease in affinity of the mutant toxin for HLA-DQ. Thus, it is likely that residues 42–48 might be involved in interaction with MHC class II molecule or mutation of these residues may induce local conformational changes that affect the MHC-binding region of the toxin. Each of these residues is conserved in SEB, [with the exception of Leu42 and Tyr83 in SpeA1 (which correspond to Leu45 and Tyr89 in SEB)] but do not appear to be involved in MHC class II binding in the SEB–DR1 complex (Figure 2C).

There are at least four alleles of SpeA: *speA1*, *speA2*, *speA3* and *speA4* (Musser *et al*., 1993). *SpeA2* and *speA3* encode for toxins that differ from SpeA1 by only one amino acid: Gly80-Ser (SpeA2), Val76-Ile (SpeA3). SpeA4 shows ~9% divergence from the other three (26 amino acid changes). SpeA1, SpeA2 and SpeA3 have been purified and examined for mitogenicity and binding to class II MHC-DQ molecules. The K_i values for SpeA1, SpeA2, and SpeA3 binding to DQ molecule are 104, 55 and 13 nM respectively. Thus, SpeA3 exhibits the highest affinity for the DQ molecule. In addition, SpeA3 is the most mitogenic of the three allelic forms to human peripheral blood mononuclear cells (PBMC) (Kline and Collins, 1996). In the SpeA1 structure, Val76 is part of the β4 strand at the interface of the N- and C-terminal domains, at the bottom of the molecule (Figure 2B and C). This residue is buried and far away from the normal SEB-like MHC class II-binding site. It should be noted that Val76 is adjacent to Asp77, a potential zinc ligand. Interestingly, when Asp77 was mutated to Ala (Hartwig and Fleischer, 1993), the resultant toxin was unable to bind MHC class II molecules. Thus, the role of this part of the SpeA1 molecule in MHC class II recognition requires further investigation.

Glycine 80 in SpeA1 corresponds to Gly86 in SEB—a residue not involved in any SEB–MHC class II interactions. It is deeply buried and located in the middle of the β4 strand, some 15 Å away from the DR1 Lys39 NZ atom (a crucial residue shown to be important in SEB–DR1 complex and conserved in both DR and DQ) in the modelled SpeA1–DR1 complex. This glycine residue adopts a conformation (ϕ = –162.3°, ψ = 169.3°) that is normally allowed for non-glycine residues, thus any mutation in this residue may not cause disruption of the main chain. However, conformation changes in this region may be induced by the presence of the Ser80 side chain

Table IV. Hydrogen-bond interactions between monomers[a] in Å

Mol1	Mol2	Mol3	Mol4
Ser43 N			Glu191 O (2.94)
OG			N (2.74)
			O (3.46)
His44 ND1			Glu189 OE1 (3.33)
Glu65 N			Glu189 OE2 (3.39)
Leu89 O		Cys90 O (2.90)	
Cys90 O		Leu89 O (2.63)	
Glu94 OE2	Gln194 N (2.57)		
	Thr193 OG1 (3.32)		
Glu189 OE1			His44 ND1 (3.36)
OE2			Gln65 N (3.03)
Glu191 N			Ser43 OG (2.81)
O			Ser43 N (3.08)
			OG (3.11)
Thr193 OG1	Glu94 OE2 (3.18)		
Gln194 N	Glu94 OE2 (2.53)		
Lys196 NZ			His44 NE2 (3.49)

[a]Cut-off 3.50 Å

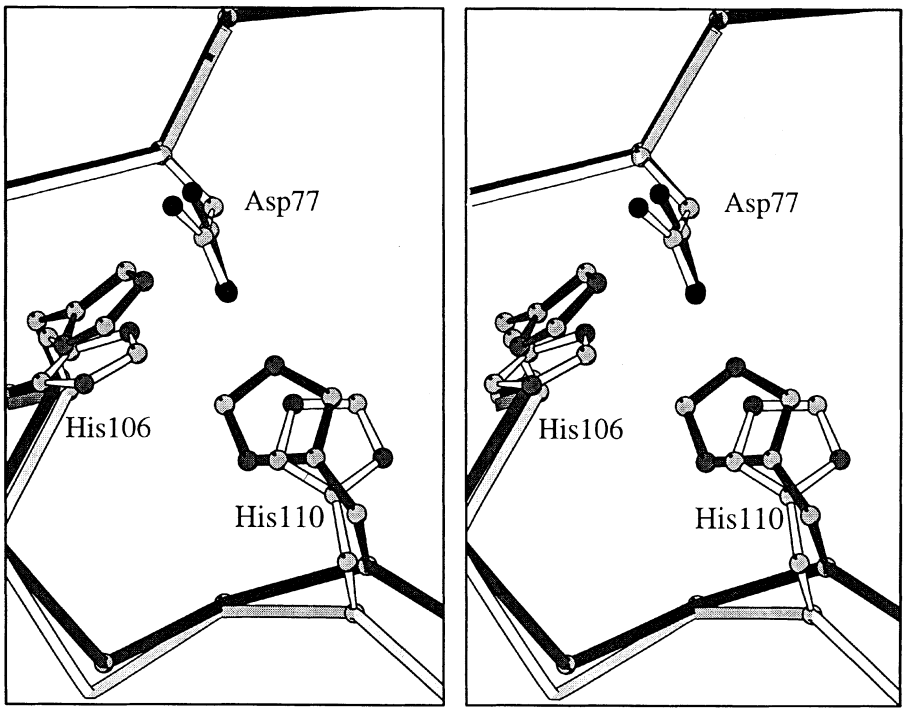

Fig. 4. Comparison of the zinc-binding site of SEC2 with the corresponding region in SpeA1. SpeA1 and SEC2 residues are shown in black and white bonds, respectively.

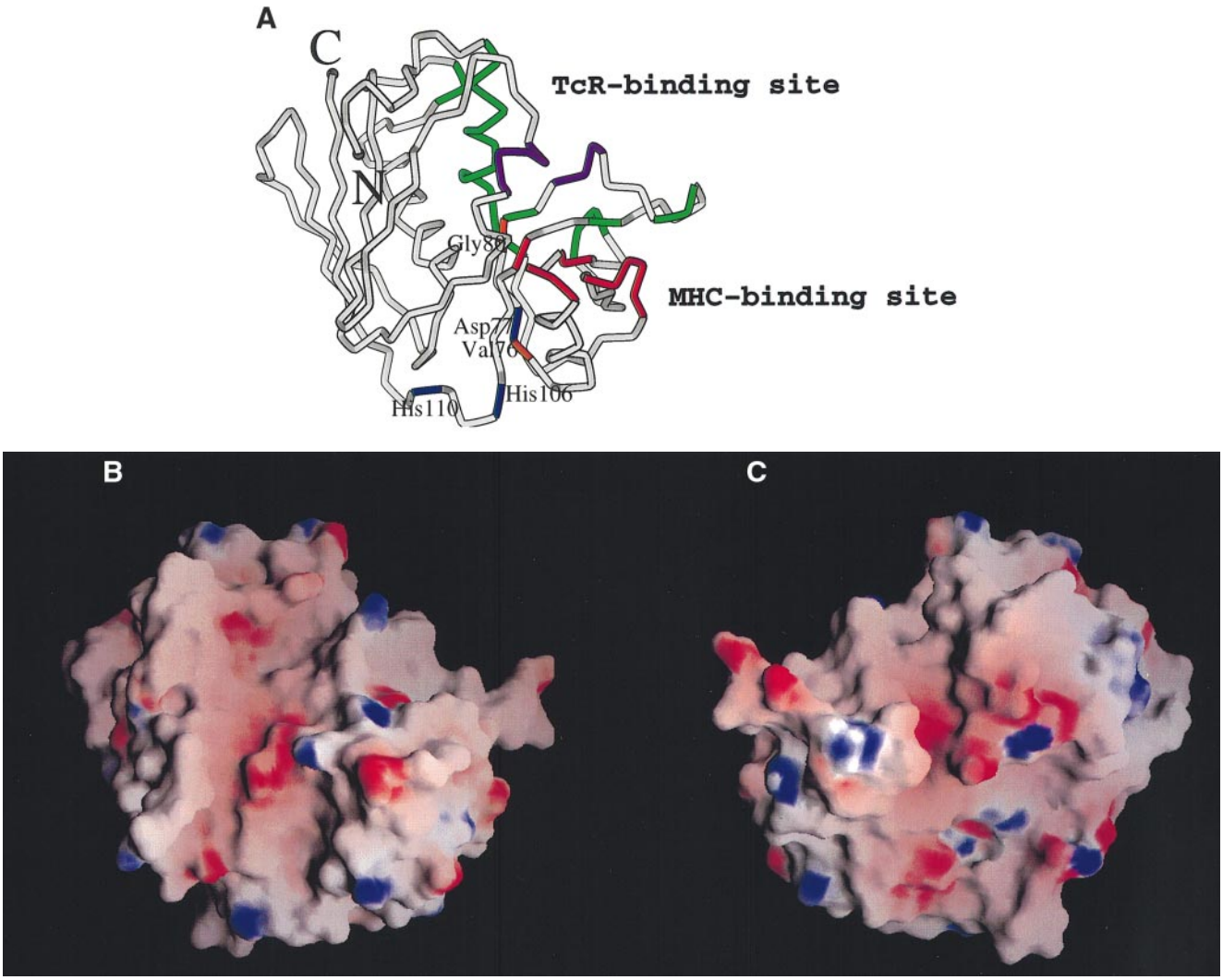

Fig. 5. (**A**) Worm representation of the SpeA1 molecule illustrating potential binding sites with MHC class II molecules and TcR. Regions implicated in MHC class II binding based on the SEB–DR1 complex structure (Jardetzky *et al*., 1994) are shown in red; Asp77, His106 and His110 which form the potential zinc-binding site in SpeA1 are shown in dark blue. Residues responsible for the different allelic forms SpeA2 and SpeA3 are shown in orange. Region implicated in both MHC- and TcR-binding are shown in purple (for details see Figure 2C). (**B** and **C**) Surface representation of SpeA1. Two views of the molecular surface of SpeA1, coloured according to the electrostatic potential from electronegative to electropositive by a red-to-blue continuous colour range. The view in (B) is the same as in (A). The view in (C) is related to that in (B) by a rotation of 180° about the vertical axis. The figure was produced using GRASP (Nicholls and Honig, 1991).

(in SpeA2). The extent of these changes is difficult to predict but it is unlikely that they would drastically change the position of other residues involved in MHC class II binding, for example Tyr83 or Tyr100 which correspond to Tyr89 and Tyr115 in SEB, respectively.

Both SpeA2 and SpeA3 differ from SpeA1 in regions away from the normal MHC class II-binding site as seen in the SEB–DR1 crystal structure. Moreover, the higher affinity of SpeA3 for DQ molecules is not easy to explain if the toxin possesses only the SEB-like MHC class II-binding site. The potential zinc-binding site of SpeA1 is, however, located in a position close to the mutation sites. If the toxin possesses a second MHC-binding site involving the zinc-binding region, the zinc ion may act as a bridge between the superantigen and the MHC class II molecule. It has been suggested that His81 of the MHC β-chain would form a potential ligand (fourth) for the zinc ion associated with SEA (Karp and Long, 1992) and possibly for SEC2 (Papageorgiou *et al*., 1995). Similar suggestions involving zinc ion-mediated interaction have been put forward for SED (Sundström *et al*., 1996) and SpeC (Roussell *et al*., 1997).

TcR-binding site

Superantigen activation of T-cells requires prior binding of the superantigen to the Vβ chain of the TcR, although each superantigen recognizes a specific Vβ subset. SpeA1 in particular activates human T-cells bearing Vβ12.2, Vβ14.1 and Vβ2.1 chains (Abe *et al*., 1991; Leonard *et al*., 1991; Tomai *et al*., 1992; Braun *et al*., 1993; Kline and Collins, 1997). Amino acid substitutions at 22 individual sites in SpeA1 have shown that each TcR Vβ requires a different combination of exotoxin residues for binding (Kline and Collins, 1997). In other words, SpeA1 utilizes different residues depending on the TcR Vβ chain presented. This has become evident from the known

superantigen structures so far, even though all of them seem to have similar three-dimensional folds but appear to have different contact residues for TcR recognition.

Direct structural information on the interactions of superantigens with the Vβ chain has been derived from the crystal structure of SEC2/SEC3–TcR Vβ complex (Fields *et al*., 1996). In the case of SpeA1, the dissociation constant for the mouse TcR Vβ8.2 is in the same range as that of SEC2 (6.2 and 7.9 μM, respectively; Malchiodi *et al*., 1995). Thus for SpeA1 in the light of structural similarities with SEC2 and mutagenesis data, the TcR-binding site appears to encompass residues from the α2 helix, β2–β3 loop, the disulfide loop, α4–β9 loop and α5 helix (Figures 2B and 5). Moreover, the Vβ12.2 and Vβ14.1 chains are phylogenetically close to mouse Vβ8.2, with five and four amino acids out of 12 being the same in the Vβ8.2 superantigen-contacting region, respectively.

From the available structural data it is clear that the TcR-contact regions of superantigens exhibit sequence variability, are located in regions of high mobility, and show considerable structural differences between toxins (Papageorgiou and Acharya, 1997). SpeA1 is not an exception. Glycine 19 in SEC2 for example is replaced by Lys16 in SpeA1 and this may affect the number of contacts with the TcR Vβ chain. An asparagine residue present in SpeA1 (Asn20), is conserved in all SEs and its critical role in TcR binding has been well established (Figure 2C). Phenylalanine 23 corresponds to Tyr26 in SEC2—a residue involved in van der Waals contacts with Gly53 of mouse TcR Vβ8.2. In SpeA1, the aromatic ring of Phe23 differs markedly from that of Tyr26 in SEC2. Tyrosine 26 is an important residue in SEC2/SEC3 and contributes to the specificity of these toxins. In SEC1, this residue is replaced by valine (Turner *et al*., 1992). A simple superposition of SpeA1 on to SEC2 (based on the SEC3–TcR Vβ complex structure; Fields *et al*., 1996) showed that Phe23 of SpeA1 points away from Gly53 of Vβ but appears to be closer to residues 66–70 (FR3 and HV4 region of Vβ).

In SEC2, four residues from the disulfide loop could make potential contacts with the complementarity-determining region 1 (CDR1) chain and Gln72 of Vβ. In the case of SpeA1, the disulfide loop is considerably shorter and it may not be able to make similar contacts. Cys90 and Cys98 of SpeA1 disulfide loop are required for stimulation of Vβ12.2-bearing T-cells (Kline and Collins, 1997). In particular, Cys90 of SpeA1 has been found to be important for stimulation of human Vβ12.2-expressing cells, but to a lesser extent for Vβ14.1-, and not at all for Vβ2.1-expressing cells (Kline and Collins, 1997). Cysteine 98 forms a disulfide bridge with Cys87. In previous studies, it was impossible to isolate a Cys87 mutant suggesting the importance of this residue in the structure of SpeA1 (Kline and Collins, 1996). Previous data have also shown that the conformation of disulfide loop between Cys87 and Cys98 is important for MHC class II binding (Kline and Collins, 1996; Roggiani *et al*., 1997). Thus, the disulfide loop appears to be involved in interactions with both MHC and TcR Vβ. Mutation of Cys98 to Ser resulted in intermediate stimulation of Vβ2.1 while the Cys90–Ser mutant had no effect on the activity of the toxin for Vβ2.1 indicating differences in the way that Vβ2.1 and Vβ12.2 bind to SpeA1 through the CDR1 regions. A modelling exercise based on the SEB–DR1 (Jardetzky *et al*., 1994) and SEC2/SEC3–TcR Vβ complexes (Fields *et al*., 1996) has demonstrated that the disulfide loop in SpeA1 needs to move towards Vβ in order to avoid steric clashes with the MHC class II molecule. Although SpeA1 and SEC2/SEC3 are closely related toxins, they bind different CDR loops of the TcR. Competition assays using peptides derived from the CDR loops of human Vβ12.2 suggest that SpeA1 interacts primarily with CDR1 and to lesser degrees with CDR2 and CDR4 (Kline and Collins, 1997). This is in contrast to SEC2/SEC3. The crystal structure of SEC2/SEC3 in complex with a mouse Vβ chain (Fields *et al*., 1996) indicates that the toxin predominantly contacts CDR2, but also interacts with CDR1 and CDR4.

The possibility that the bound antigen peptide may affect the formation of the TcR–superantigen–MHC trimolecular complex (in this case with SpeA1) can not be ruled out. It has been shown that presentation of different superantigens to MHC class II molecules can be affected by the bound peptide (Thibodeau *et al*., 1994). Moreover, from the available structural data, it appears that interactions of MHC β-chain and the Vα chain are plausible (Fields *et al*., 1996; Papageorgiou and Acharya, 1997; Figure 6). The proximity of the disulfide loop to the antigen-binding groove also needs to be considered. Thus, the superantigen activity may be further modulated by small changes in the orientation of each component of the complex. This may contribute to better optimization of the contacts by utilization of different subsets of residues. As recently reported by Leder *et al*. (1998), changes in the affinity for TcR can be compensated by changes on the affinity of the MHC component of the complex.

SpeA1 superantigen recognition

The toxin SpeA1 crystallizes with four molecules in the asymmetric unit. These molecules do not form intermolecular disulfide bridges (the closest that free cysteines are found between any pair of monomers is 6Å). The buried surface area between monomer pairs involve mainly electrostatic interactions and the toxin appears to be a monomer in solution. A possible model for the interaction of SpeA1 monomer with MHC class II and TcR molecules are shown in Figure 6. This is assisted by the previously determined SEB–DR1 (Jardetzky *et al*., 1994) and SEC2/SEC3–Vβ and αβ structures (Fields *et al*., 1996; Garcia *et al*., 1996). The modelled complex depicts the normal mode of MHC class II (as in the case of SEB) and TcR recognition. However, based on available mutagenesis data on SpeA1, it is possible that the toxin may utilize an alternative MHC class II-binding site, involving recognition through the zinc ion. Experiments to establish the definitive role of zinc ion in SpeA1 are in progress.

Superantigen dimerization as a prerequisite for T-cell activation has been suggested for SED (Sundström *et al*., 1996) and SpeC (Roussell *et al*., 1997). In these superantigens, the presence of zinc ions in distinct parts of the molecule results in the formation of different types of dimers. In SED, the zinc-binding site at the C-terminal domain of the toxin cross-links two SED molecules and consequently each molecule binds an MHC class II molecule by utilizing the SEB-like MHC class II-binding site. In SpeC, dimerization occurs through a zinc ion at

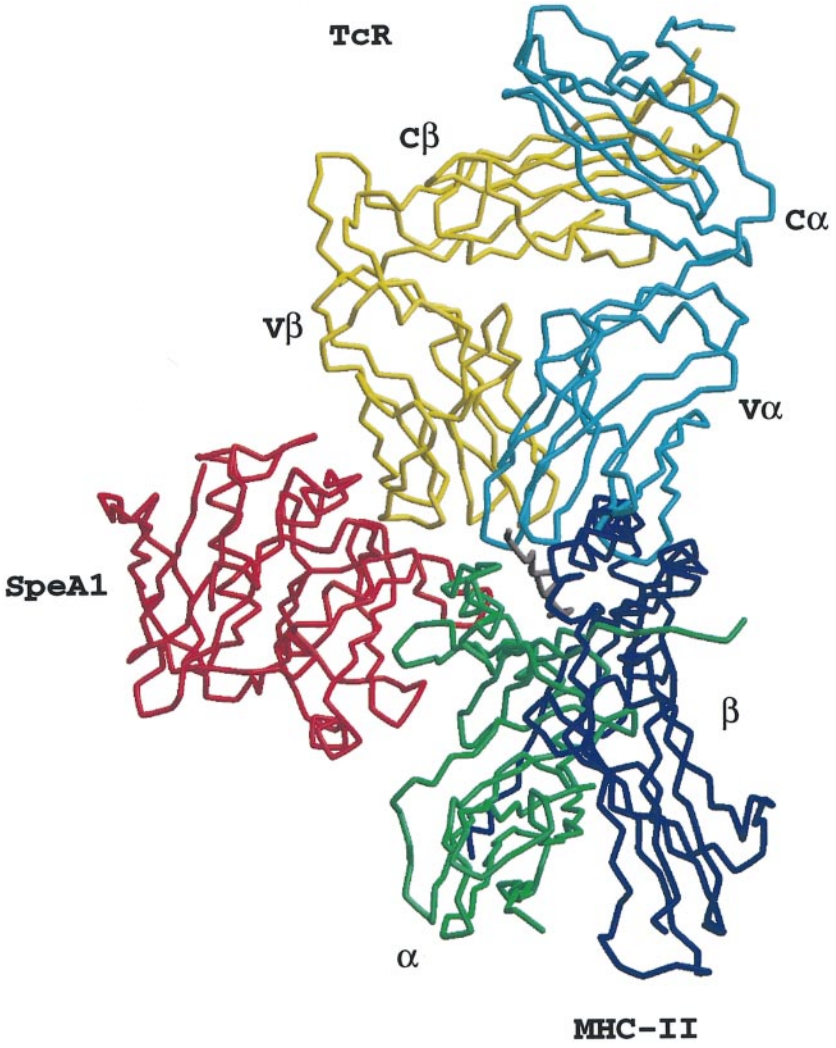

Fig. 6. Proposed model for MHC–SpeA1–TcR ternary complex based on the crystal structures of SEB–DR1 (Jardetzky *et al.*, 1994; PDB accession code: 1SEB), the TcR Vβ–SEC2 complex (Fields *et al.*, 1996; PDB accession code: 1JCK) and the TcR αβ structure (Garcia *et al.*, 1996; PDB accession code: 1TCR).

the normal MHC-binding site, and MHC binding involves the zinc-binding site at the C-terminal domain. There is high degree of correlation between SpeC structure and solution experiments (Li *et al.*, 1997). The involvement of dimerization in superantigen function needs to be explored further. It should be mentioned that higher order oligomerization of the TcR play an integral part in the TcR-signalling complex (Germain, 1997; Davis *et al.*, 1998) and hence, superantigens may have adapted themselves to this mechanism of TcR clustering (Proft and Fraser, 1998).

Preliminary experiments with SpeA1 indicate that this toxin would also have evolved to act as a dimer under certain conditions. Preparations of SpeA1 purified from *Escherichia coli* with pH 7.9 buffers show ~50% toxin monomer and 50% toxin dimer forms (see Materials and methods). The SDS–PAGE analysis indicated that the dimer is disulfide linked (C.M.Collins, unpublished results). The zinc ion does not seem to have an effect on dimer formation. The toxin purified at pH 7.9 was separated into monomer and dimer forms by gel-filtration chromatography. Monomer and dimer preparations were tested for the ability to stimulate human PBMC, and there was no detectable difference in activity between the preparations (C.M.Collins, unpublished results). Thus both SpeA1 dimers and monomers are biologically active. Even though the present SpeA1 structure (determined from the material purified at pH 5.7, a monomer in solution) does not lend support for an inter-molecular disulfide-bridge formation, it is tempting to speculate that in the dimeric form, the flexible disulfide loop might undergo local structural rearrangement to allow formation of an inter-molecular disulfide bridge involving Cys90. This would allow the possibility of bivalent TcR binding. If this proves to be correct, SpeA1 will provide yet another mechanism for TcR recognition. Structural and biochemical studies to establish the biological relevance of dimer formation are currently in progress.

Concluding remarks

The crystal structure of SpeA1, a member of the bacterial superantigen family has been determined at 2.6 Å resolution to an R_{cryst} of 19.4%. Comparison with other staphylococcal and streptococcal superantigens shows a high degree of structural similarity, in particular with SEC2. A potential zinc-binding site was identified in the

structure at the interface between the N- and C-terminal domains in a similar position to that of SEC2 zinc-binding site. Possible binding modes for the toxin with MHC class II molecules and TcRs are proposed based on (i) the existence of three allelic forms of the toxin and (ii) the presence of the potential zinc-binding site. The structural data has provided a clear view of the various residues involved in SpeA1–TcR interactions previously identified by mutagenesis. The data obtained here are the first step in the design and development of compounds, such as TcR-specific peptides, to interfere with the SpeA1–TcR interaction, and in turn prevent SpeA from acting as a superantigen. It is possible that compounds that can specifically block the superantigenic properties of SpeA might prove useful as therapies to ameliorate and possibly prevent STSS in an infected individual. However, in order to understand the specific details of T-cell stimulation by SpeA and other related superantigens, the urgent need for structural details of the MHC–SpeA–TcR complex and for further functional studies cannot be over-emphasized.

Materials and methods

Protein expression and purification

SpeA1 was expressed as a fusion protein with an N-terminal histidine-rich leader sequence using the pET expression and purification system of Novagen, Madison, WI. The bacterial expression vector pET15b was utilized for these experiments. The recombinant toxin was expressed in *E.coli* BL21 (DE3) (Novagen, Madison, WI) and purified by metal chelation chromatography on 'His-bind' resin at pH 7.9 as described by the manufacturer. Under these conditions the resulting toxin preparation contained both a monomer and a dimer form. To inhibit dimer formation, the metal chelation column-binding buffer (5 mM imidazole, 0.5 M NaCl, 20 mM Tris–HCl), elution buffer (1 M imidazole, 0.5 M NaCl, 20 mM Tris–HCl), and wash buffer (60 mM imidazole, 0.5 M NaCl, 20 mM Tris–HCl) were adjusted to pH 5.7. The toxin used in the present crystallographic study was prepared at pH 5.7 and was >95% monomer.

Recombinant toxin eluted from the His-bind resin was cleaved with thrombin, and the histidine-rich leader peptide separated from the toxin by dialysis against phosphate-buffered saline (PBS). After thrombin cleavage, four amino acids from the leader peptide remain fused to the N-terminus of SpeA1 (Gly-Ser-His-Met). Thrombin was removed from the toxin preparation by chromatography over *p*-amino benzamidine agarose (Sigma Chemicals, St Louis, MO). Toxin was then dialysed against PBS, 0.14 M NaCl, 2.7 mM KCl, 5.4 mM Na_2HPO_4 and 1.8 mM KH_2PO_4 and concentrated with Centricon-10 filter units (Amicon).

Plasma emission analysis

The metal content in SpeA1 (0.5 mg per sample) was analysed using a Jarrell-Ash 965 ICP Plasma Emission Spectrophotometer. Analysis was performed at the Chemical Analysis Laboratory, University of Georgia Research Services, University of Georgia, USA.

Crystallization and data collection

Crystals of SpeA1 were grown at 16°C by the vapour diffusion hanging drop method. Initial crystallization trials produced rod-like crystals after mixing 2 µl of SpeA1 (~10 mg/ml) with an equal volume of a reservoir solution containing 20% PEG 3350, 20% isopropanol and 0.1 M sodium cacodylate buffer at pH 6.5. However, due to the irregular growth of these crystals, alteration of the crystallization conditions was necessary. Crystals with identical morphology but of better quality were grown using 17% PEG 8000, 0.2 M ammonium sulphate, 0.1 M sodium cacodylate buffer at pH 6.5. Micro-seeding techniques were employed to increase the size of the crystals for X-ray structure analysis.

A data set to 2.9 Å resolution was first collected from one crystal on station PX 9.5 of the Synchrotron Radiation Source, Daresbury, UK. Forty-seven images were collected (1.5° oscillation, 200 s exposure time) using a 30-cm MAR Research image plate operated in the small MAR mode (18 cm diameter). Data processing was performed with the HKL package (Otwinowski and Minor, 1997) and the systematic absences found to agree with an orthorhombic $P2_12_12$ space group. The final R_{merge} was 13.7% with an overall completeness of 95% and a multiplicity of 4.5. A second data set to 2.6 Å resolution was collected on station BW7B in EMBL Hamburg (c/o DESY) from a single crystal grown in the presence of ammonium sulfate. The station was equipped with a MAR345 image plate and data were collected using the small MAR mode (18 cm). The exposure time was 30 s per image and the oscillation range was 1°. One hundred and three images were collected. Processing, scaling and merging was accomplished with the HKL package. Details of the data processing are given in Table I. The two data sets, although isomorphous, were not merged as they were obtained from crystals grown under different conditions.

Structure determination

The 2.9 Å data set was used for the initial structure determination and the 2.6 Å data set was used in the final refinement (Table I). Attempts to solve the structure by molecular replacement with the program AMoRe (Navaza, 1994) using a homology model based on the structures of SEB (1.5 Å; Papageorgiou *et al*., 1998) and SEC2 (2.0 Å; Papageorgiou *et al*., 1995) were unsuccessful even though SEB and SEC2 share 53 and 49% sequence identity with SpeA1. Moreover, a polyalanine model of SEB was also unable to locate the first SpeA1 molecule. However, by using a polyalanine model of SEC2 (<20% of the scattering power) and by excluding a number of residues from the N-terminal tail and the highly flexible disulfide loop, a promising peak in the rotation function was obtained, 1.2σ higher than the next one (resolution 3.0 Å, box size 75.5×68.8×55.8 Å). Subsequently, in the translation function, this peak resulted in a correlation coefficient of 29.9% and an *R*-factor of 53.8%, after rigid body refinement using AMoRe. Examination of this solution on the graphics using the program 'O' (Jones *et al*., 1991) revealed good packing and no stereochemical clashes with symmetry-related molecules. Due to the presence of four molecules in the asymmetric unit, the position of the first molecule was fixed in the translation search for the remaining molecules. The second molecule (second peak in the translation function), after rigid body refinement, gave values of 37 and 51.4% for the correlation coefficient and *R*-factor respectively. After fixing the two molecules, these values improved to 44 and 49% when the third molecule was identified. Surprisingly, the fourth molecule could not be located. However, its position was identified by examination of the electron-density map and the crystal contacts between the other three molecules. An anchor point was found close to Met199 and this was used for the construction of a five-residue stretch from the fourth molecule. After one round of preliminary refinement, the rest of the fourth molecule was eventually located.

Refinement

The solution from AMoRe was subjected to rigid body refinement using X-PLOR 3.851 (Brünger, 1992b). At this stage, side chains were not included in the refinement and in the electron density map calculations. However, map averaging using the program DM from the CCP4 program suite (Collaborative Computational Project, No. 4, 1994) permitted the incorporation of most of the sidechains in the model according to the amino acid sequence. The refinement procedure included alternate cycles of simulated annealing at moderate temperatures (typically 1000 K) and manual rebuilding. The progress of refinement was monitored using the free *R*-factor (R_{free}) with 5% of the reflections set aside and not included in the refinement (Brünger, 1992a). Initial refinement was carried out using the 2.9 Å data set. Due to the high R_{merge} value in the outer shell, only reflections to 3.0 Å were used initially but, as the refinement progressed, the resolution was extended to 2.9 Å and the R_{free} value did not increase. The starting values of R_{cryst} and R_{free} for the three molecules were 48.6 and 49.2% and a round of positional refinement improved the values to 42.9 and 45.8%, respectively. Inclusion of the fourth molecule, a solvent bulk correction (reflections 40.0–3.0 Å) and a slow cool protocol starting at 1000 K resulted in an R_{cryst} of 29.9% and an R_{free} of 33.2%. Extension of the refinement to 2.57 Å was achieved with the new data set, in 0.1 Å steps, using molecular dynamics at 1000 K followed by Powell energy minimization. Overall B-factor refinement followed by individual temperature factor refinement, was employed after the R_{cryst} dropped below 29% with data from 20.0–2.57 Å. Tight non-crystallographic restraints (200 kcal/mol·Å^2) were applied throughout the refinement but were relaxed at the later stages and finally released altogether. Water molecules were identified using the program ARP (Lamzin and Wilson, 1997) and examined on the graphics before inclusion in the refinement. Water molecules with temperature factors above 60 Å^2 after one round of refinement were excluded from the model and subsequent refinement. Engh and Huber stereochemical target values were used throughout the refinement (Engh and Huber, 1991).

The final refinement statistics are presented in Table I. Map calculations were performed with programs from the CCP4 suite using all the reflections in the resolution range 20.0–2.57 Å. Final atomic co-ordinates of SpeA1 will be deposited in the Brookhaven Protein Data Bank.

Accession number

The atomic coordinates of SpeA1 have been deposited with the Brookhaven Protein Data Bank under the accession code 1B1Z.

Acknowledgements

We thank the staff at the Synchrotron radiation sources at Daresbury (UK) and EMBL outstation at Hamburg (HASYLAB, c/o DESY, Germany), Dr Demetres Leonidas and Ms Evangelia Chrysina for their help with X-ray data collection. We also thank Dr Daniel Holloway for the constructive criticisms of the manuscript. This work was supported by the Medical Research Council (UK) Programme Grant (9540039) to K.R.A., in part by a PHS grant (AI 42353) from the National Institutes of Health (USA) to C.M.C. and the European Union through its support of the work at EMBL, Hamburg, through the HCMP Access to Large Installations Project (Contract CHGE-CT93-0040).

References

Abe,J., Forrester,J., Nakahara,T. and Lafferty,J.A. (1991) Selective stimulation of human T cells with streptococcal erythrogenic toxins A and B. *J. Immunol.*, **146**, 3747–3750.

Acharya,K.R., Passalacqua,E.F., Jones,E.Y., Harlos,K., Stuart,D.I., Brehm,R.D. and Tranter,H.S. (1994) Structural basis of superantigen action inferred from crystal structure of toxic-shock syndrome toxin-1. *Nature*, **367**, 94–97.

Barton,G.J. (1993) ALSCRIPT – a tool to format multiple sequence alignments. *Protein Eng.*, **6**, 37–40.

Bohach,G.A., Fast,D.J., Nelson,R.D. and Schlievert,P.M. (1990) Staphylococcal and streptococcal pyrogenic toxins involved in toxic shock syndrome and related illnesses. *Crit. Rev. Microbiol.*, **17**, 251–272.

Braun,M.A., Gerlach,D., Hartwig,U.F., Ozegowski,J.H., Romagne,F., Carrel,S., Kohler,W. and Flesicher,B. (1993) Stimulation of human T cells by streptococcal 'superantigen' erythrogenic toxins (scarlet fever toxins). *J. Immunol.*, **150**, 2457–2466.

Brünger,A.T. (1992a) Free *R* value: a novel statistical quantity for assessing the accuracy of crystal structures. *Nature*, **355**, 472–474.

Brünger,A.T. (1992b) *X-PLOR: Version 3.1. A system for crystallography and NMR*. Yale University, New Haven, CT.

Collaborative Computational Project, No. 4 (1994) The CCP4 suite: programs for protein crystallography. *Acta Crystallogr.*, **D50**, 760–763.

Davis,M.M., Boniface,J.J., Reich,Z., Lyons,D., Hampl,J., Arden,B. and Chien,Y.-h. (1998) Ligand recognition by αβ T cell receptors. *Annu. Rev. Immunol.*, **16**, 523–544.

Engh,R.A. and Huber,R. (1991) Accurate bond and angle parameters for X-ray protein structure refinement. *Acta Crystallogr.*, **A47**, 392–400.

Esnouf,R.M. (1997) An extensively modified version of Molscript that includes greatly enhanced coloring capabilities. *J. Mol. Graph.*, **15**, 132–134.

Fields,B.A., Malchiodi,E.L., Li,H., Ysern,X., Stauffacher,C.V., Schlievert,P.M., Karjalainen,K. and Mariuzza,R.A. (1996) Crystal structure of a T-cell receptor β-chain complexed with superantigen. *Nature*, **384**, 188–192.

Garcia,K.C., Degano,M., Stanfield,R.L., Brunmark,A., Jackson,M.R., Peterson,P.A., Teyton,L. and Wilson,I.A. (1996) An αβ T cell receptor structure at 2.5 Å and its orientation in the TCR–MHC complex. *Science*, **274**, 209–219.

Germain,R.N. (1997) T-cell signalling: the importance of receptor clustering. *Curr. Biol.*, **7**, 640–644.

Hartwig,U.F. and Fleischer,B. (1993) Mutations affecting MHC class II binding of the superantigen streptococcal erythrogenic toxin A. *Eur. J. Immunol.*, **5**, 869–875.

Hartwig,U.F., Gerlach,D. and Fleischer,B. (1994) Major histocompatibility complex class II binding site for streptococcal pyrogenic (erythrogenic) toxin A. *Med. Microbiol. Immunol.*, **183**, 257–264.

Hauser,A.R., Stevens,D.L., Kaplan,E.L. and Schlievert,P.M. (1991) Molecular analysis of pyrogenic exotoxins from *Streptococcus pyogenes* isolates associated with toxic shock-like syndrome. *J. Clin. Microbiol.*, **29**, 1562–1567.

Herman,A., Kappler,J.W., Marrack,P. and Pullen,A.M. (1991) Superantigens—mechanism of T-cell stimulation and role in immune responses. *Annu. Rev. Immunol.*, **9**, 745–772.

Hoffmann,M.L., Jablonski,L.M., Crum,K.K., Hackett,S.P., Chi,Y.-I., Stauffacher,C.V., Stevens,D.L. and Bohach,G.A. (1994) Predictions of T-cell receptor- and major histocompatibility complex- binding sites on staphylococcal enterotoxin C1. *Infect. Immun.*, **62**, 3396–3407.

Hoge,C.W., Schwartz,B., Talkington,D.F., Breiman,R.F., Macneill,E.M. and Englender,S.J. (1993) The changing epidemiology of invasive group A streptococcal infections and the emergence of streptococcal toxic shock-like syndrome—A retrospective population-based study. *J. Am. Med. Assoc.*, **269**, 384–389.

Jardetzky,T.S., Brown,J.H., Gorga,J.C., Urban,R.G., Chi,Y.I., Stauffacher,C., Strominger,J.L. and Wiley,D.C. (1994) Three-dimensional structure of a human class II histocompatibility molecule complexed with superantigen. *Nature*, **368**, 711–718.

Jones,T.A., Zou,J.Y, Cowan,S.W. and Kjeldgaard,M. (1991) Improved methods for building protein models in electron density maps and the location of errors in these models. *Acta Crystallogr.*, **A47**, 110–119.

Kabsch,W. and Sander,C. (1983) Dictionary of protein secondary structure: pattern recognition of hydrogen-bonded and geometrical features. *Biopolymers*, **22**, 2577–2637.

Karp,D.R. and Long,E.O. (1992) Identification of HLA-DR1 β chain residues critical for binding staphylococcal enterotoxins A and E. *J. Exp. Med.*, **175**, 415–424.

Kim,J., Urban,R.G., Strominger,J.L. and Wiley,D.C. (1994) Toxic shock syndrome toxin-1 complexed with a class II major histocompatibility molecule HLA-DR1. *Science*, **266**, 1870–1874.

Kline,B.J. and Collins,C.M. (1996) Analysis of the superantigenic activity of mutant and allelic forms of streptococcal pyrogenic exotoxin A. *Infect. Immun.*, **64**, 861–869.

Kline,B.J. and Collins,C.M. (1997) Analysis of the interaction between the bacterial superantigen streptococcal pyrogenic exotoxin A (SpeA) and the human T-cell receptor. *Mol. Microbiol.*, **24**, 191–202.

Kotb,M. (1998) Superantigens of Gram-positive bacteria: structure–function analyses and their implications for biological activity. *Curr. Opin. Microbiol.*, **1**, 56–65.

Lamzin,V.S. and Wilson,K.S. (1997) Automated refinement for protein crystallography. *Methods Enzymol.*, **277**, 269–305.

Laskowski,R.A., MacArthur,M.W., Moss,D.S. and Thornton,J.M. (1993) PROCHECK: a program to check the stereochemical quality of protein structures. *J. Appl. Crystallogr.*, **26**, 283–291.

Leder,L. *et al.* (1998) A mutational analysis of the binding of staphylococcal enterotoxins B and C3 to the T cell receptor β chain and major histocompatibility complex class II. *J. Exp. Med.*, **187**, 823–833.

Leonard,B.A.B., Lee,P.K., Jenkins,M.K. and Schlievert,P.M. (1991) Cell and receptor requirements for streptococcal pyrogenic exotoxin T-cell mitogenicity. *Infect. Immun.*, **59**, 1210–1214.

Li,H., Llera,A. and Mariuzza,R.A. (1998) Structure–function studies of T-cell receptor–superantigen interactions. *Immunol. Rev.*, **163**, 177–186.

Li,P.L., Tiedemann,R.E., Moffat,S.L. and Fraser,J.D. (1997) The superantigen streptococcal exotoxin C (SPE-C) exhibits a novel mode of action. *J. Exp. Med.*, **186**, 375–383.

Malchiodi,E.L., Eisenstein,E., Fields,B.A., Ohlendorf,D.H., Schlievert, P.M., Karjalainen,K. and Mariuzza,R.A. (1995) Superantigen binding to a T cell receptor β chain of known three-dimensional structure. *J. Exp. Med.*, **182**, 1833–1845.

Marrack,P. and Kappler,J. (1990) The staphylococcal enterotoxins and their relatives. *Science*, **248**, 705–711.

Merritt,E.A. and Murphy,M.E.P. (1994) Raster3D version 2.0: a program for photo realistic molecular graphics. *Acta Crystallogr.*, **D50**, 869–873.

Murzin,A.G., Brenner,S.E., Hubbard,T. and Chothia,C. (1995) SCOP – A structural classification of protein database for the investigation of sequences and structure. *J. Mol. Biol.*, **247**, 536–540.

Musser,J.M., Hauser,A.R., Kim,M.H., Schlievert,P.M., Nelson,K. and Selander,R.K. (1991) Streptococcus pyogenes causing toxic-shock-like syndrome and other invasive diseases: clonal diversity and pyrogenic exotoxin expression. *Proc. Natl Acad. Sci. USA*, **88**, 2668–2672.

Musser,J.M., Nelson,K., Selander,R.K., Gerlach,D., Huang,J.C., Kapur,V. and Kanjilal,S. (1993) Temporal variation in bacterial disease frequency: molecular population genetic analysis of scarlet fever epidemics in Ottawa and in Eastern Germany. *J. Infect. Dis.*, **167**, 759–762.

Navaza,J. (1994) AMoRe: an automated package for molecular replacement. *Acta Crystallogr.*, **A50**, 157–163.

Nelson,K., Schlievert,P.M., Selander,R.K and Musser,J.M. (1991) Characterization and clonal distribution of 4 alleles of the *spea* gene encoding pyrogenic exotoxin-A (scarlet fever toxin) in *Streptococcus pyogenes*. *J. Exp. Med.*, **174**, 1271–1274.

Nicholls,A. and Honig,B. (1991) A rapid finite difference algorithm, utilising successive over relaxation to solve the Poisson–Boltzmann equation. *J. Comput. Chem.*, **12**, 435–445.
Otwinowski,Z. and Minor,W. (1997) Processing of X-ray diffraction data collected in oscillation mode. *Methods Enzymol.*, **276**, 307–326.
Papageorgiou,A.C. and Acharya,K.R. (1997) Superantigens as immunomodulators: recent structural insights. *Structure*, **5**, 991–996.
Papageorgiou,A.C., Acharya,K.R., Shapiro,R., Passalacqua,E.F., Brehm,R.D. and Tranter,H.S. (1995) Crystal structure of the superantigen enterotoxin C2 from *Staphylococcus aureus* reveals a zinc-binding site. *Structure*, **3**, 769–779.
Papageorgiou,A.C., Brehm,R.D., Leonidas,D.D., Tranter,H.S. and Acharya,K.R. (1996) The refined crystal structure of toxic shock syndrome toxin-1 at 2.07 Å resolution. *J. Mol. Biol.*, **260**, 553–569.
Papageorgiou,A.C., Tranter,H.S. and Acharya,K.R. (1998) Crystal structure of microbial superantigen staphylococcal enterotoxin B at 1.5 Å resolution: implications for superantigen recognition by MHC class II molecules and T-cell receptors. *J. Mol. Biol.*, **277**, 61–79.
Prasad,G.S., Earhart,C.A., Murray,D.L., Novick,R.P., Schlievert,P.M. and Ohlendorf,D.H. (1993) Structure of toxic shock syndrome toxin-1. *Biochemistry*, **32**, 13761–13766.
Proft,T. and Fraser,J. (1998) Superantigens: just like peptides only different. *J. Exp. Med.*, **187**, 819–821.
Read,R.J. (1986) Improved coefficients for map calculation using partial structures with errors. *Acta Crystallogr.*, **A42**, 140–149.
Roggiani,M., Stoehr,J.A., Leonard,B.A.B. and Schlievert,P.M. (1997) Analysis of toxicity of streptococcal pyrogenic exotoxin A mutants. *Infect. Immun.*, **65**, 2868–2875.
Roussell,A., Anderson,B.F., Baker,H.M., Fraser,J.D. and Baker,E.N. (1997) Crystal structure of the streptococcal superantigen SPE-C: dimerization and zinc-binding suggest a novel mode of interaction with MHC class II molecules. *Nature Struct. Biol.*, **4**, 635–643.
Schad,E.M., Zaitseva,I., Zaitsev,V.N., Dohlsten,M., Kalland,T., Schlievert,P.M., Ohlendorf,D.H. and Svensson,L.A. (1995) Crystal structure of the superantigen staphylococcal enterotoxin type A. *EMBO J.*, **14**, 3292–3301.
Schad,E.M., Papageorgiou,A.C., Svensson,L.A. and Acharya,K.R. (1997) A structural and functional comparison of staphylococcal enterotoxins A and C2 reveals remarkable similarity and dissimilarity. *J. Mol. Biol.*, **269**, 270–280.
Stevens,D.L. (1995) Streptococcal toxic-shock syndrome–spectrum of disease, pathogenesis and new concepts in treatment. *Emerg. Infect. Dis.*, **1**, 69–78.
Stuart,D.I., Levine,M., Muirhead,H. and Stammers,D.K. (1979) The crystal structure of cat pyruvate kinase at a resolution of 2.6 Å. *J. Mol. Biol.*, **134**, 109–142.
Sundström,M., Abrahmsén,L., Antonsson,P., Mehindate,K., Mourad,W. and Dohlsten,M. (1996) The crystal structure of staphylococcal enterotoxin type D reveals Zn^{2+}-mediated homodimerization. *EMBO J.*, **15**, 6832–6840.
Swaminathan,S., Furey,W., Pletcher,J. and Sax,M. (1992) Crystal structure of staphylococcal enterotoxin B, a superantigen. *Nature*, **359**, 801–806.
Swaminathan,S., Furey,W., Pletcher,J. and Sax,M. (1995) Residues defining Vβ specificity in staphylococcal enterotoxins. *Nature Struct. Biol.*, **2**, 680–686.
Thibodeau,J., Cloutier,I., Lavoie,P.M, Labrecque,N., Mourad,W., Jardetzky,T. and Sékaly,R.-P. (1994) Subsets of HLA-DR1 molecules defined by SEB and TSST-1 binding. *Science*, **266**, 1874–1878.
Tomai,M.A., Schlievert,P.M. and Kotb,M. (1992) Distinct T-cell receptor Vβ gene usage by human T lymphocytes stimulated with the streptococcal pyrogenic exotoxins and pep M5 protein. *Infect. Immun.*, **60**, 701–705.
Turner,T.N., Smith,C.L. and Bohach,G.A. (1992) Residues 20, 22 and 26 determine the subtype specificities of staphylococcal enterotoxins C1 and C2. *Infect. Immun.*, **60**, 694–697.

Received July 2, 1998; revised September 10, 1998; accepted October 28, 1998

Note added in proof

Based on a preliminary soaking experiment with zinc, we can now confirm that SpeA1 binds zinc in the crystal (in all four molecules) as described in this article.